論　文

The Effect of Wind Turbine Sitting on the Power Output and Flow Fields of Offshore Wind Farms

Jay Prakash GOIT[*1]　　Asim ÖNDER[*2]

[*1] Dept. of Mechanical Engineering, Kindai University Hiroshima 739-2116, Japan
E-mail: jay.goit@hiro.kindai.ac.jp
[*2] Dept. of Marine Environment and Engineering, National Sun Yat-sen University, Kaohsiung 80424, Taiwan
E-mail: asim.onder@mail.nsysu.edu.tw

Abstract

The effect of interaction between wake generated by wind turbines is particularly significant in offshore wind farms, because the turbulence in the ambient flow is low, thus, the wind turbine wake diffuses at the slower rate with the surrounding flow. As a result, efficiency of wind farms strongly depends on the turbine spacing inside the farm. The current study investigates the effect of wind turbine sitting on the flow fields and performance of offshore wind farms. To that end, large eddy simulations (LES) are performed for seven different wind farm layouts (three aligned and four staggered) with varying turbine spacing and number, while the farm area is same for all the cases. Better wake recovery is observed for the staggered layouts, and this can be attributed to the larger streamwise spacing for this layout. However, the spanwise averaged wind speeds are lower for the staggered layout indicating that more power is extracted by the wind farm from the flow. Spanwise-averaged turbulence kinetic energy increases downstream inside the aligned farm, while it remains roughly the same after the second turbine row. This is because the staggered layout is able to induce evenly distributed turbulence from the upstream region. In terms of power output, it is found that for the same wind farm area, power output of staggered wind farm can be as high as 30 to 40%.

Keywords : Offshore wind farm, Wind turbine layout, Atmospheric boundary layer, Large-eddy simulation

1. Introduction

Offshore wind energy has been experiencing a promising growth in both established wind energy markets of Europe and the emerging markets of Asia. While the current share of offshore wind is around 7% (only 57 GW compared to 780 GW of onshore turbine) of the total cumulative wind power generation, the Global Wind Energy Council (GWEC) report states that with 21.1 GW of newly commissioned wind turbine in 2021, the annual installation rate increased by three times[1]. The primary motivation behind offshore wind energy development is that the offshore sites are generally characterized by higher and uniform wind speeds leading to higher capacity factors. However, in large wind farms, the performance of wind turbines is governed by the interactions of wakes generated by individual turbines as well as the two-way interaction between wind farms and the atmospheric boundary layer (ABL)[2]. Wake interactions in the entrance region of wind farms lead to the drop in wind speed and in turn substantial drop in power generation at downstream turbine rows[3,4]. The effect of wake interactions is particularly significant in offshore wind farms. This is because the turbulence in the ambient flow is low, thus, the wind turbine wake diffuses at the slower rate with the surrounding flow. Although in the fully developed region that follows the entrance region, energy extracted by wind turbines is replenished by the turbulent entrainment of kinetic energy flux from above the wind farm[5,6], for the full recovery of the wind speed in the wake, wind turbines have to be placed significantly far apart. Since the efficiency of wind farms depends on turbine sitting, in the current study we investigate the effect of wind turbine layout on the flow fields and power output of wind farms.

Large-eddy simulations (LES) have been the primary tools for investigating flow structures inside wind farms, though wind tunnel experiments with model wind turbine arrays have also provided valuable validating data on flow statistics and evolution of wind farm boundary layers[7-9]. Earlier LES studies considered infinitely large wind farms in a fully developed wind-farm boundary layer and mainly discussed about vertical entrainment of kinetic energy from above the wind farm[5,6]. Later studies which have simulated for finite - sized wind farms, have investigated entrance effect[10], atmospheric stability[11], interaction between very-large-scale motions and turbines[12], effect of coastal terrain on the performance of a nearshore offshore wind farms[13] and so on. More recently, LES data is also being compared against the measurement from actual wind farms (see e.g. Sood *et al.*[14]). The reader is referred to Porte-Agel *et al.*[2] or other recent reviews of the wind farm flows for the details.

Regarding the effect of turbine spacing and array configuration on wake interaction and power outputs,

*1 近畿大学工学部 機械工学科（〒739-2116 広島県東広島市高屋うめの辺 1 番）E-mail: jay.goit@hiro.kindai.ac.jp
*2 国立中山大学 海洋環境及び工学系 (〒80424 高雄市台湾)
（原稿受付： 2023 年　3 月　7 日）

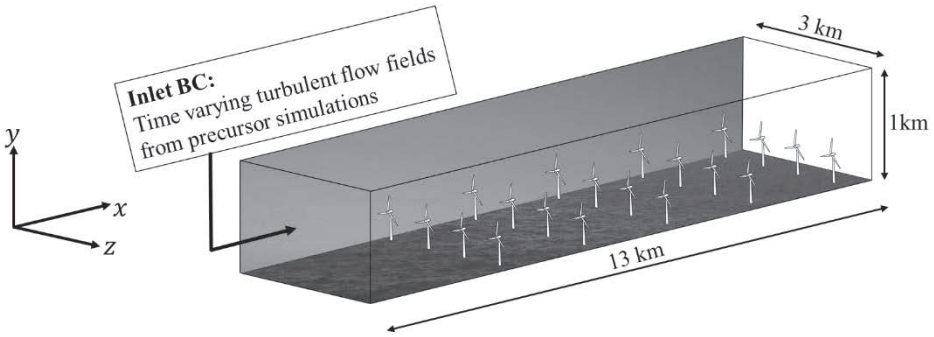

Fig. 1 Schematic of the computation domain with aligned wind farm layout. Note that the figure shows fewer turbines than the actual simulation cases in Table 1.

research efforts have been made both using wind tunnel experiments[15] and LESs[16]. However, more studies on wind farm layout are necessary to understand the relation between efficient layouts and their interaction with the ABL. Therefore, in this study we aim to investigate the effect of wind turbine sitting on the power output and flow fields in offshore wind farms. To that end, the area of the wind farm is fixed and several layouts with varying turbine numbers are analysed using large-eddy simulations. As far as the authors are aware, earlier studies have not investigated the effect of wind turbine layouts on the overall performance and flow fields of wind farm of the given area. The study therefore, is important from the engineering point of view, since any farm layout can only be defined over the pre-allotted leased land or leased zone (for offshore) area. The paper is further organized as follows: Sec. 2 describes the LES framework and simulation cases. Sec. 3 presents results and discussions, describing the flow fields followed by power outputs of all the layouts. The main conclusions are summarized in Sec. 4.

2. Methodology and simulation cases

The open source CFD software OpenFOAM[17], is employed to perform LES of a neutrally stratified ABL. The governing flow equations are the filtered Navier-Stokes equations given by:

$$\frac{\partial \tilde{u}_i}{\partial x_i} = 0 \tag{1}$$

$$\frac{\partial \tilde{u}_i}{\partial t} + \frac{\partial}{\partial x_j}\left(\tilde{u}_i \tilde{u}_j\right) = -\frac{1}{\rho}\frac{\partial \tilde{p}}{\partial x_i} + \nu \frac{\partial^2 \tilde{u}_i}{\partial x_j^2} + \frac{\partial \tau_{ij}}{\partial x_j} + f_i \tag{2}$$

where $\tilde{u}_i = [\tilde{u}_1, \tilde{u}_2, \tilde{u}_3]$ is the resolved velocity field corresponding to streamwise, vertical and spanwise directions, $\tilde{p}$ is the pressure field, ρ is the air density, ν is kinematic viscosity and τ_{ij} is the subgrid-scale stress. The term f_i represents the force exerted by wind turbine on the flow field. The wall-adapting local eddy-viscosity (WALE) model is employed to model the effect of subgrid-scale stresses on the resolved flow fields. Further details about the simulation tool is available in Goit & Önder[13].

Force due to the wind turbine is modelled using the actuator-disk model (ADM) in which the axial force induced by a wind turbine on the flow is uniformly distributed over a permeable disk. This axial force ($\mathrm{F_t}$) is defined using the characteristic thrust coefficient (C_T) of a turbine

$$\mathrm{F_t} = \frac{1}{2} C_T \rho U_0^2 A_d \tag{3}$$

where U_0 is a free stream velocity and A_d is a rotor surface area. Since it is not easy to find the free stream velocity for downstream turbines in a wind farm, we derived a method for projecting U_0 from the wind speed at the disk. The source code and further description of the ADM are available in the git repository[18].

Table 1. Summary of the simulations cases. S_x and S_z are streamwise and spanwise spacings. dS_z is spanwise distance between the rotor center of two consecutive turbine rows in staggered wind farms.

Case	Layout	Spacing	No. of turbines
1	Aligned	$S_x = 5D,\ S_z = 5D$	65
2	Aligned	$S_x = 7D,\ S_z = 5D$	50
3	Aligned	$S_x = 9D,\ S_z = 5D$	40
4	Staggered	$S_x = 5D$, $S_z = 5D$, $dS_z = 2.5D$	65
5	Staggered	$S_x = 7D$, $S_z = 5D$, $dS_z = 2.5D$	50
6	Staggered	$S_x = 7D$, $S_z = 5D$, $dS_z = 1D$	50
7	Staggered	$S_x = 9D$, $S_z = 5D$, $dS_z = 2.5D$	40

Figure 1 shows the schematic of the computation domain. The size of the computation domain is $\mathrm{L}_x \times \mathrm{L}_y \times \mathrm{L}_z = 13\mathrm{km} \times 1\mathrm{km} \times 3\mathrm{km}$. Here $\mathrm{L}_x, \mathrm{L}_y$ and L_z are streamwise, vertical and spanwise lengths. A uniform structured grid is employed, and grid resolutions in streamwise, vertical and spanwise directions are $\mathrm{dx} \times \mathrm{dy} \times \mathrm{dz} = 10\ \mathrm{m} \times 5\ \mathrm{m} \times 8\ \mathrm{m}$ resulting in the total number of grid points of 97.5×10^6. In this study, following boundary conditions are imposed.

1. *inlet:* time varying turbulent flow fields generated in a separate precursor simulation
2. *outlet:* zero-gradient for the velocity and fixed value for the pressure
3. *top:* slip condition for velocity and zero-gradient for pressure

4. *spanwise:* periodic boundary conditions
5. *bottom surface:* wall stress model which is a function of the velocity field at the first vertical grid point and the surface roughness height. The offshore surface is modelled by imposing the roughness height, $y_0 = 0.001$ m.

The precursor simulation has a domain size of $L_x \times L_y \times L_z = 15\text{km} \times 1\text{km} \times 3\text{km}$ and uses the same grid resolution as the wind farm simulations. It also employs the same roughness height of $y_0 = 0.001$ m. Both streamwise and spanwise boundary conditions are periodic, and the simulation is driven by a constant pressure gradient. The precursor setup of the current study is same as those in Goit and Önder[13]. Therefore, readers are referred to that work for the further description and validation of the LES model.

Simulation are performed for seven wind farm layouts as summarized in Table 1. Note that cases 4, 5 and 7 are regular staggered wind farms with turbines exactly in between the two upstream and downstream turbines, while in case 6 turbines are staggered by $1D$ in the spanwise direction compared to the upstream and downstream turbines. Rotor diameter (D) is 120 m. For the better comparison of the farm power, the area of the wind farm is approximately same for all the cases. This is the reason why there are more turbines in cases 1 and 4, while fewer turbines in cases 3 and 7. Wind farm area of all, but cases 1 and 4 is $7.56 \times 3 = 22.68$ km^2. The farm area of Cases 1 and 4 is $7.2 \times 3 = 21.6$ km^2.

3. Results and Discussions

3.1 Flow fields

Flow fields from simulations of wind farm layouts listed in Table 1 are discussed first. Figure 2 shows the instantaneous streamwise velocity fields for cases 2, 5 and 6 from the hub height plane. Note that the streamwise turbine spacing for these three cases is $7D$. It can be appreciated that the near wake fields show similar characteristics for both the aligned and the staggered layouts. In case 2 (aligned layout), wind turbine wakes form discrete streamwise columns which extend over the entire farm length. Additionally, high speed flow can be observed passing between turbine columns. In other two cases (especially case 5), wind speeds upstream of each turbine are relatively higher. This is due to larger streamwise spacing between consecutive turbines. Staggered configuration allows better exploitation of the incoming flow. As a result, wind speed is more evenly distributed deep inside the wind farm, and there is no presence of streamwise-elongated high- and low-speed columns.

Figure 3 shows the time-averaged streamwise velocity fields in the vertical planes along the rotor center. We have shown the statistics for cases 2 and 5 in this and other contours below. As with the instantaneous velocity fields, mean velocities are also higher upstream of turbines in the staggered case. Development of the farm-induced internal boundary layer (IBL) from the first turbine row is clearly observed in both the contours. However, the difference in the IBL thicknesses is not significant for the two cases. Wind speeds do not seem to recover in the wake of wind farms in either of the layouts. Note that the streamwise length from the last turbine row to the end of the domain is 20D.

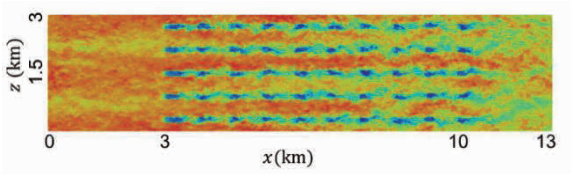

(a) Case 2: Aligned ($S_x = 7D,\ S_z = 5D$)

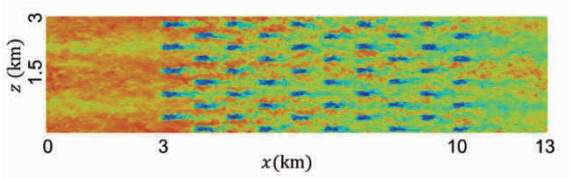

(b) Case 5: Staggered ($S_x = 5D,\ S_z = 5D,\ dS_z = 2.5D$)

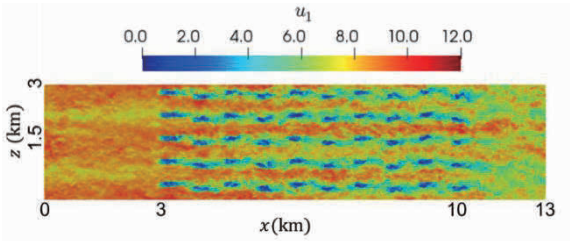

(c) Case 6: Staggered ($S_x = 7D,\ S_z = 5D,\ dS_z = 1D$)

Fig. 2 Instantaneous streamwise velocity fields at the hub height planes for aligned (case 2), staggered (case 5) and staggered (case 6) in Table 1. The velocity contours are presented in m/s.

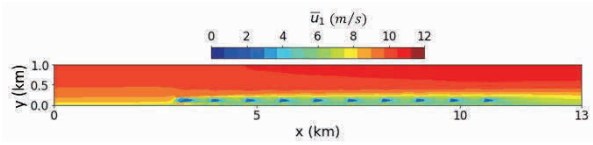

(a) Case 2

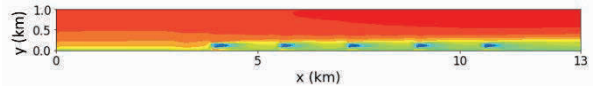

(b) Case 5

Fig. 3 Contours of the mean streamwise velocity in vertical planes along the rotor center.

Comparison of streamwise velocity profiles at the rotor center in Figure 4(a) shows better wake recovery for the staggered layout (case 5), even though inflow velocity is almost same for the two cases. This is due to larger streamwise spacing between consecutive turbines in the staggered farm. Interestingly, wind speed is even higher than the inflow velocity at the upstream turbine row of staggered farm. This happens because the turbines in the first row (see Figure 2(b)) acts as a blockage to the incoming flow, and thus accelerating the flow between two adjacent turbines.

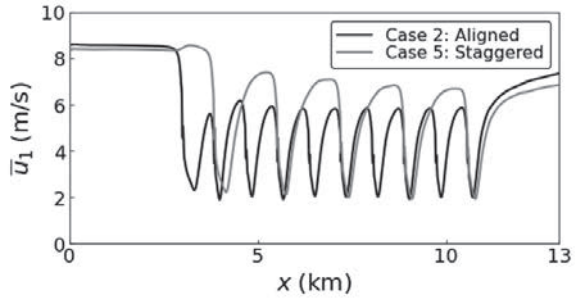

(a) At the rotor center

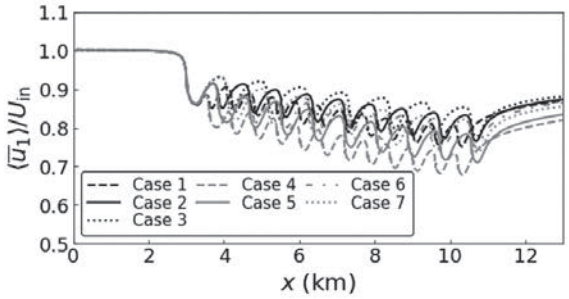

(b) Averaged over entire spanwise extent of the domain

Fig. 4 Comparison of the streamwise evolution of the mean velocity.

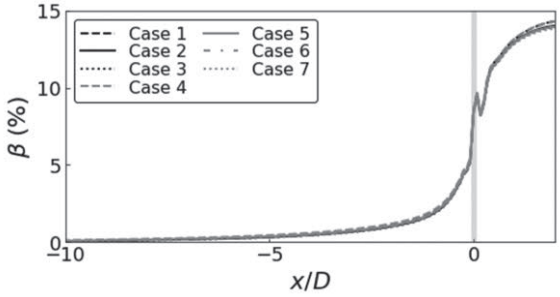

Fig. 5 Farm-induced blockage for all seven cases to the incoming flow. Vertical line is the position of the first turbine row.

Figure 4(b) shows streamwise profiles at hub height averaged over the spanwise length of the domain for all seven layouts. Wind speeds are normalized by inflow wind speed (U_{in}). Unlike the wind speed at the rotor center, spanwise-averaged velocities are lower for the staggered layouts. This indicates that in aggregate staggered farm extracts more power from the ABL. Wind speeds in the wake of the wind farm, i.e., downstream from the last turbine row, are also significantly lower for the staggered cases. It is obvious that the drop in wind speeds is the largest for closely packed layouts (cases 1 and 4). However, wind speeds inside even the closely spaced rectangular layout are mostly higher compared to all four staggered layouts considered in this study. This is due to higher power extracted by staggered layouts from the flow fields. Note that even though same precursor data is used as the inflow conditions in all seven simulations, wind speeds upstream of wind farm are different for those cases. This is due to the smaller domain length (3 km) upstream of the farm. Longer streamwise length is required upstream of the farm to reduce the farm-imposed blockage and maintain closer upstream wind speeds for all the layouts. Future extensions of the present work will consider longer upstream sections.

Figure 5 shows the wind farm-induced blockage to the incoming flow. In this study blockage (β) is defined as:

$$\beta = \frac{U_{\text{inflow}} - \overline{u}_1}{U_{\text{inflow}}} \times 100 \ \ (\%) \tag{4}$$

where U_{inflow} is the upstream inflow wind speed averaged over the spanwise length and is taken 20D upstream from the first turbine row. Farm layout has no noticeable effect on the blockage, and β profiles are almost same for all simulation cases. Although we have not performed simulation by varying turbine number in the spanwise direction, we believe blockage will mostly depend on the spanwise turbine density of the first row facing the incoming flow. Blockage values for the current layouts are around 3%, 1% and 0.35% respectively at 0.5D, 2D and 5D upstream of the wind farm. Further upstream blockage is negligibly small.

Figure 6 shows mean turbulent kinetic energy (TKE, $\overline{k} = \frac{1}{2}\overline{u'_\iota u'_\iota}$), and shear stress ($-\overline{u'_1 u'_2}$) in the streamwise-vertical plane along the rotor center. In the staggered case, both TKE and shear stress in the wake reduce significantly before reaching the downstream turbines. This is also due to larger streamwise spacing in the staggered layout. These quantities are further discussed using the streamwise evolution of their profiles in the following figures.

Figure 7 compares the TKE profiles of aligned (case 2) and staggered (case 5) layouts averaged over the spanwise length. The figure also shows the dispersive TKE profiles ($\langle \overline{k}'' \rangle = \frac{1}{2}\langle \overline{u}_\iota'' \overline{u}_\iota'' \rangle$) which arise from the spatial inhomogeneity caused by the presence of wind farm. Definitions of dispersive TKE and dispersive stresses are described in Goit & Önder[13]. The spanwise-averaged TKE increases downstream inside the aligned wind farm, while the profile remains roughly same in the staggered farm. Staggered layout induces evenly distributed turbulence right from the second turbine row and that is maintained throughout the wind farm. In the upstream region of aligned farm, the turbulence level is higher in the turbine columns, but the level is lower in the channel between the columns. However, downstream inside the farm, TKE gets more evenly distributed with enhanced mixing of the flow fields. This is reflected in the dispersive TKE which is higher upstream in the aligned wind farm, but gradually decreases downstream inside the farm. Dispersive TKE is always lower for the staggered wind farm.

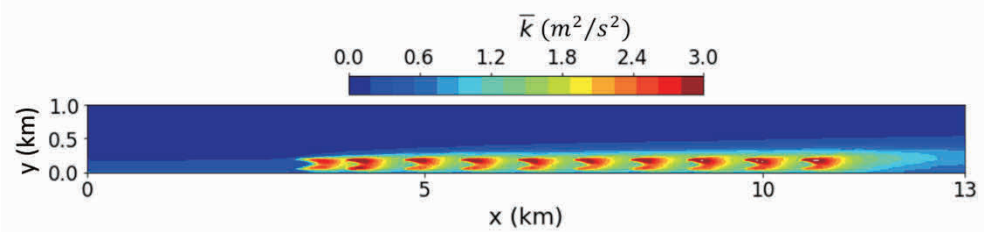

(a) Turbulence kinetic energy (case 2)

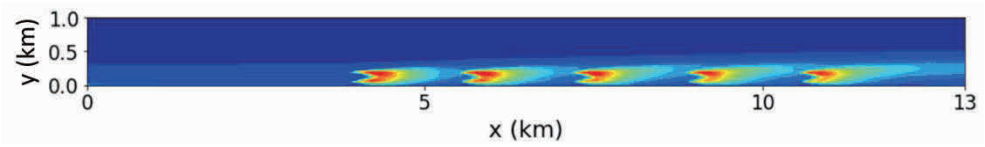

(b) Turbulence kinetic energy (case 5)

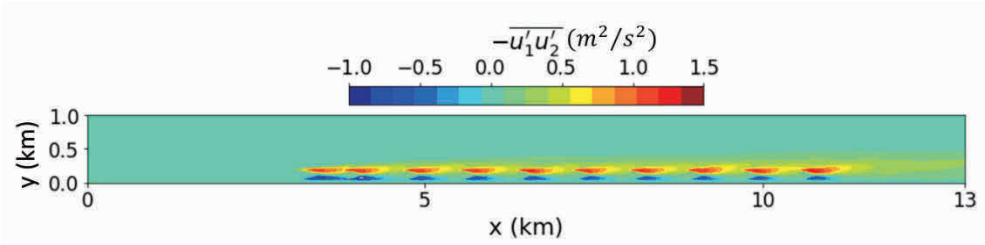

(c) Shear stress (case 2)

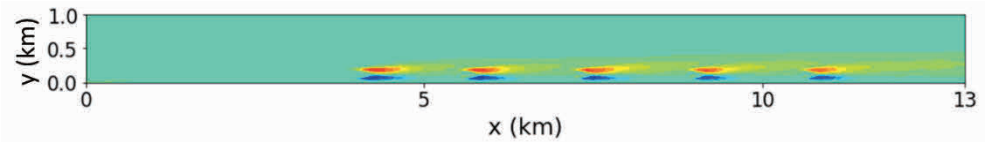

(d) Shear stress (case 5)

Fig. 6 Turbulence statistics in the streamwise vertical plane along the rotor center. The contours are presented in m^2/s^2.

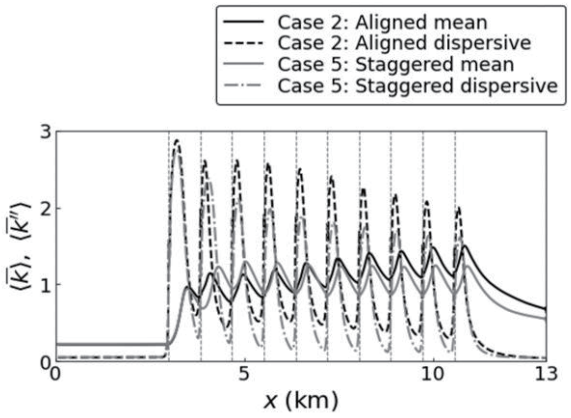

Fig. 7 Streamwise evolution of turbulent kinetic energy at the hub height plane, averaged over the spanwise extent of the domain. Vertical dashed lines indicate the location of wind turbine row.

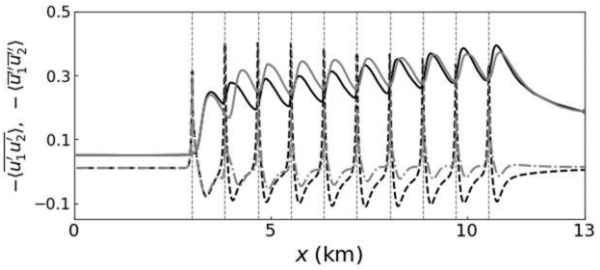

(a) Reynolds shear stress

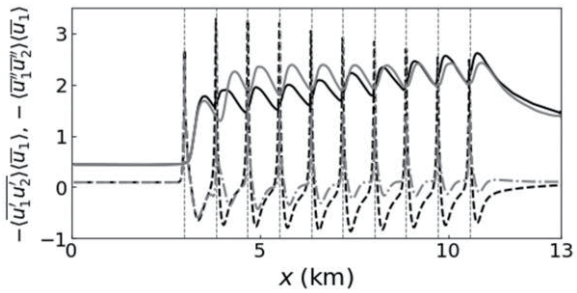

(b) Vertical kinetic energy flux

Fig. 8 Streamwise evolution of Reynolds shear stress and vertical kinetic energy flux at the rotor top tip. Profiles are averaged over the spanwise extent of the domain and legends are the same as in Figure 7.

In large wind farms, energy has to be entrained from the flow above the farm, since the kinetic energy of the inflow wind is rapidly depleted in the first few rows. The entrainment phenomenon is quantified using Reynolds shear stress and vertical kinetic energy flux. Figure 8 shows shear stresses, vertical kinetic energy fluxes and corresponding dispersive profiles at the turbine top-tip level averaged over the spanwise length of the domain. Mean shear stresses and kinetic energy fluxes for both aligned and staggered layouts increase downstream inside the farm, suggesting that the energy entrainment and the farm power production have not reached the equilibrium state even for the last turbine rows. Both quantities are larger in the staggered layouts for the first seven rows, after which profiles of the aligned layout become larger. Dispersive stresses and fluxes have sharp peaks at turbine rows but rapidly drop in the wake regions. Magnitude of dispersive quantities are lower for the staggered layout.

3.2 Farm power output

Since mean wind speeds and energy entrainments differ for different layouts, power output should also vary with the farm layout. Power output of the layouts in Table 1 are discussed next.

Figure 9 shows the time-and row-averaged power outputs as a function of turbine row. Power outputs of four aligned layouts are compared in Figure (a), while those of staggered layouts are compared in Figure (b). The power has been normalized by the power of the first turbine row of case 2, which is considered as a reference case. Both in aligned and staggered layouts, power output of the row decreases with decreasing turbine spacing. The effect of streamwise spacing is most significant in the second row of the aligned farm. For cases 1 and 2, power outputs in the second row drop before increasing slightly in the third row. For the staggered layouts, second rows generate higher power than the first rows. As discussed earlier, this is because the blockage due to the first turbine row results in the higher wind speed at the second row, and ultimately resulting in higher power outputs from this row. It can be appreciated that the staggered layouts generate higher power than the aligned layouts for the given streamwise spacing. However, row-wise power outputs from both layouts tend to converge for downstream rows. For example, when streamwise spacing is 7D, normalized power outputs of the 10th row for all three layouts (cases 2, 5 and 6) is around 0.5. Therefore, one can expect that in large wind farms (with more than 10 rows), whether the turbines are placed in staggered or aligned configuration is less important for the later rows, instead streamwise spacing will only decide their performance.

Figure 10 shows total farm power output of all seven layouts for the total simulation time of 2 h 46 min. Total wind farm powers are normalized by the power of the case 2. Staggered wind farm with the smallest turbine spacing (case 4) resulted in the highest power output which is 40% higher compared to the reference power of case 2. Power output of case 5 which has same number of turbines as well as same streamwise spacing as case 2 is 30% higher. Among the aligned layouts, case 1 with the largest number of turbines generates the highest power. But it is still low compared to all staggered layouts. Even though power outputs increase with the number of turbines, reducing the turbine spacing will result in the drop in the capacity factors of downstream turbines (see Figure 9). This in turn will increase the cost of energy from such wind farm and possibly make them economically less feasible. Therefore, while performing layout analysis of wind farm, in addition to the total farm power output, performance of individual turbines should also be take into account, so that the levelized cost of energy (LCOE) is lower enough to generate sufficient profit.

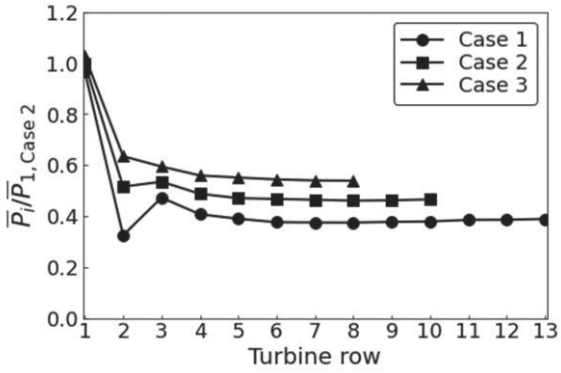

(a) Aligned cases

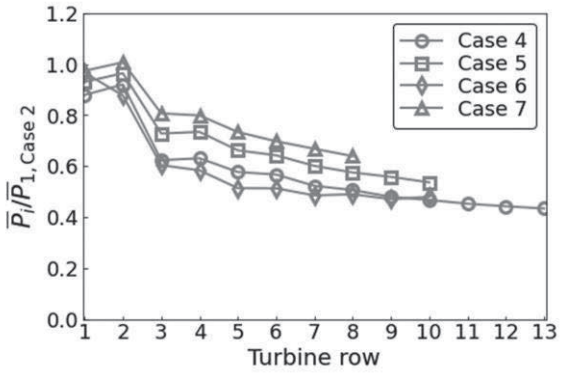

(b) Staggered cases

Fig. 9 Comparison of time and row-averaged power outputs.

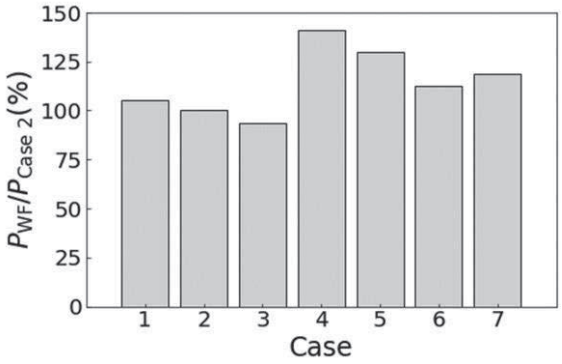

Fig. 10 Comparison of the total farm power outputs.

Note that this study only considers a single fixed wind direction. In real wind farms, changing wind directions is inevitable, and this will result in the variation in the farm layout with respect to the incoming flow, thus, making the

analysis of the flow statistics way more complicated. The total farm power estimation will also drop compared to the ideal case of this study. Therefore, in actual layout optimization of a potential wind energy development site, distribution of wind speed and wind direction for the period of one year should be taken into account. One data-based approach can be to perform simulations for a large number of layouts and then couple them with wind speed and direction distribution to determine most efficient wind farm layout for the given site. Since the computational resources have been more accessible and cheaper in the recent years, the method is feasible, and the resulting layout can be expected to perform better than the wind farm layout designed using wake models which is a common approach in the wind energy industry.

4. Conclusions

In this study we have investigated the effect wind farm layout on the flow fields and performance of offshore wind farms. To that end, seven different layouts (three aligned and four staggered) were defined by varying streamwise spacing, spanwise arrangement and the number of turbines, while maintaining the same wind farm area for all the cases. Wind farm simulations were performed using LES.

Evaluation of velocity fields showed better wake recovery for the staggered layout, even though the inflow velocity and turbulence were almost same for all the cases. This was attributed to the larger streamwise spacing in the staggered layouts. However, spanwise-averaged wind speeds were lower for the staggered layouts. Furthermore, for the farm layouts considered in this study, there was no noticeable difference in the blockage to the incoming flow. Analysis of turbulence showed that average TKE increased downstream inside the aligned wind farm, while it remained roughly the same in the staggered farm. This was because the staggered layout was able to induce evenly distributed turbulence from the upstream region. Both mean shear stresses and kinetic energy fluxes in the rotor top tip region increased downstream for the aligned and staggered alignment, suggesting that the energy entrainment and the farm power production did not reach the equilibrium for the current wind farm size.

Power outputs of aligned wind farms were smaller than the staggered layout. For the same wind farm area, total power outputs from fully staggered layouts (cases 4 and 5) were 30 to 40% higher than the aligned cases. However, the current study only considered a single wind direction. In the future work, we plan to take into account annual distribution of wind speed and wind direction of a potential wind energy development site, and couple the simulations with layout optimization scheme.

Acknowledgements

Jay Prakash Goit acknowledges Electric Technology Research Foundation of Chugoku for supporting this work. The computations were performed on Oakbridge-CX supercomputer system.

References

1) Lee, J., Zhao, F., *Global Wind Report*, Global Wind Energy Council (GWEC), Brussels, Belgium, 2022.
2) Porté-Agel, F., Bastankhah, M., Shamsoddin, S., Wind-Turbine and Wind-Farm Flows: A Review, *Boundary-Layer Meteorology*, Vol. 174, 2020, pp.1-59.
3) Barthelmie, R. J., Frandsen, S. T., Hansen K. et al., Modelling the Impact of Wakes on Power Output at Nysted and Horns Rev, In the proceeding of the *European Wind Energy Council (EWEC)*, 2009, pp.1-10.
4) Wu, Y. T., Porté-Agel, F., Simulation of Turbulent Flow Inside and Above Wind Farms: Model Validation and Layout Effects, *Boundary-Layer Meteorology*, Vol. 146, 2013, pp.181-205.
5) Calaf, M., Meneveau, C., Meyers, J., Large Eddy Simulation Study of Fully Developed Wind-turbine Array Boundary Layers, *Physics of Fluids*, Vol. 22, 2010, pp.015110.
6) Goit, J. P., Meyers, J., Optimal Control of Energy Extraction in Wind-farm Boundary Layers, *Journal of Fluid Mech*anics, Vol. 768, 2015, pp.5-50.
7) Chamorro, L. P., Porté-Agel, F., Turbulent flow inside and above a Wind Farm: A Wind-tunnel Study, *Energies*, Vol. 4 2011, pp.1916-1936.
8) Hamilton, N., Cal, R. B., Anisotropy of the Reynolds Stress Tensor in the Wakes of Wind Turbine Arrays in Cartesian Arrangements with Counter-rotating Rotors, *Physics of Fluids*, Vol. 27, 2015, pp.015102.
9) Segalini, A., Chericoni, M., Boundary-layer Evolution over Long Wind Farms, *Journal of Fluid Mechanics*, Vol. 925, 2021, pp.A2 1-29.
10) Goit, J. P., Munters, W., Meyers, J., Optimal Coordinated Control of Power Extraction in LES of a Wind Farm with Entrance Effects, *Energies*. Vol. 9, No. 29, 2016, pp.1-20.
11) Ghaisas, N. S., Archer, C. L., Xie, S., Wu, S., Maguire, E., Evaluation of Layout and Atmospheric Stability Effects in Wind Farms Using Large-eddy Simulation, *Wind Energy*, Vol. 20, 2017, pp.1227-1240.
12) Önder, A., Meyers, J., On the Interaction of Very-large-scale Motions in a Neutral Atmospheric Boundary Layer with a Row of Wind Turbines, *Journal of Fluid Mechanics*, Vol. 841, 2018, pp.1040-1072.
13) Goit, J. P., Önder, A., The Effect of Coastal Terrain on Nearshore Offshore Wind Farms: A Large-eddy Simulation Study, *Journal of Renewable and Sustain Energy*, Vol. 14, 2022, pp.043304.
14) Sood, I., Simon, E., Vitsas, A., Blockmans, B., Larsen, G. C., Meyers, J., Comparison of Large Eddy Simulations against Measurements from the Lillgrund Offshore Wind Farm, *Wind Energy Science*, Vol. 7, No. 6, 2022, pp.2469-2489.
15) Hamilton, N., Tutkun, M., Cal, R. B., Wind Turbine Boundary Layer Arrays for Cartesian and Staggered Configurations: Part II, Low-dimensional Representations via the Proper Orthogonal Decomposition, *Wind Energy*, Vol. 18, No. 2, 2014, pp.297-315.
16) Stevens, R. J. A. M., Gayme, D. F., Meneveau, C., Effects of Turbine Spacing on the Power Output of Extended Wind-farms, *Wind Energy*, Vol. 19, 2016, pp.359-370.
17) ESI. OpenFOAM. https://www.openfoam.com/. Accessed 18 July, 2022.
18) Önder, A., Goit, J. P., windTurbineModels: an OpenFOAM package with basic wind turbine models for wind farm simulations, https://github.com/asimonder/windTurbineModels, Accessed 8 March, 2022.